

Mapping the X-ray Emitting Ejecta in Cassiopeia A with Chandra

Una Hwang (1,2), Stephen S. Holt (1), & Robert Petre (1)

(1) *NASA Goddard Space Flight Center, Greenbelt, MD 20771,*

(2) *Department of Astronomy, University of Maryland, College Park, MD 20742*

ABSTRACT

We present X-ray emission line equivalent width images of the bright Galactic supernova remnant Cassiopeia A for the elements Si, S, Ar, Ca, and Fe using a 50,000 s observation with the Advanced CCD Imaging Spectrometer on the Chandra X-ray Observatory. The images essentially identify the bulk of detectable ejecta of these elements over a wide range of surface brightness, and show morphologies distinctly different from that of the broadband X-ray emission and of the 4-6 keV continuum emission. The Si, S, Ar, and Ca maps, while different in turn from those of Fe, show that these X-ray emitting ejecta are distributed similarly to the fast optical ejecta knots, and clearly delineate the X-ray counterpart of the northeast optical jet. Low surface brightness regions just outside the bright shell in the north and west are also shown to have strong line emission. The strong Fe emission is exterior to that of other elements in the east, as previously noted, but is generally coincident elsewhere. The projected interior has relatively little emission traced by high line equivalent widths.

1. Introduction

A record of a supernova explosion is imprinted in the spatial distribution of ejecta in the remnant, but then is gradually erased by dynamic interaction with the surrounding medium. Cassiopeia A, the brightest and youngest known Galactic remnant, is one of the best targets for study of the ejecta distribution. Detailed observations and modelling at optical wavelengths (e.g., Reed et al. 1995, Lawrence et al. 1995, Fesen & Gunderson 1996) show a complex system of chemically enriched knots with high velocities that form a shell with a linear extension to the northeast called the jet. Although these ejecta are nearly undecelerated, they show asymmetries in their red- and blue-shifted velocities and in their line intensity ratios that arise from their interaction with an inhomogeneous medium.

Optical emission, however, accounts for only a small fraction of the total mass, as typical shocks in young supernova remnants heat the bulk of the mass to X-ray emitting temperatures. X-ray spectral imaging, which is required to identify and map these ejecta, has been carried out most extensively with the ASCA Observatory (e.g., Holt et al. 1994, Fujimoto et al. 1995, Hwang & Gotthelf 1997; also Vink et al. 1999 with SAX). The moderate spectral resolution of the ASCA

CCD detectors allows strong line blends of individual elements to be imaged with the 3' half-power diameter point spread function of the ASCA mirrors. With the launch of the Chandra X-ray Observatory comes a tremendous increase in the capability to make these observations. The Chandra mirrors provide $< 0.5''$ imaging capability, which is on par with excellent ground-based optical observations, while the Advanced CCD Imaging Spectrometer (ACIS) on Chandra gives spectral resolution comparable to that of the ASCA CCDs.

Cas A was the Chandra first light target in 1999 August, and Hughes et al. (2000) use this early observation to note the existence of Fe-dominated zones in the east that are exterior to Si-dominated zones. Because Fe is synthesized in the innermost layers of the star, this is interpreted as an overturning of ejecta layers in this region during the explosion.

In this paper, we present the global distribution of the X-ray line emission in Cas A using a new Chandra observation that is ten times longer than any previous one with ACIS. We account for the locally variable underlying continuum to produce maps of the line-to-continuum ratio that reveal the distribution of strong line emission throughout the remnant over a wide range of surface brightness. These are the first such images that have been produced for X-ray emission from all these elements in any young supernova remnant.

2. Emission Line Images

Cas A was observed on 2000 January 30-31 using the backside illuminated ACIS chip S3 for 50,000 s in graded mode (i.e., each event is assigned a grade on board the spacecraft, rather than in later processing, that is based on the local pixel intensity distribution in the 3.24 s readout cycle). Only the standard ASCA grade 02346 events are retained. The light curve is stable, and in any case the source count rate is much higher than the background contribution. Some 16 million photons were collected during the observation, which was carried out at a CCD operating temperature of -120 C.

The ACIS spectrum obtained for the entire remnant is shown in Fig. 1. It features prominent He α ($n=2 \rightarrow n=1$) blends of Si, S, Ar, and Ca, plus emission from L and K transitions of Fe, and a weak Mg blend that is further blended with Fe L emission. The spectrum at lower energies is strongly attenuated by the high column density of neutral hydrogen towards Cas A. The ACIS spectrum is comparable to that obtained by ASCA (e.g., Holt et al. 1994), except that the ACIS S3 blends the weak Ly α lines with the stronger He α emission.

We selected photons corresponding to a particular spectral feature by identifying appropriate pulse height ranges, as indicated in Fig. 1. Except for Fe, we combine the He α and Ly α emission of each element in a single image. We do not include Mg in this paper because it is both blended with Fe L and highly absorbed. We have made no correction for the spatially varying gain across the CCD, as this effect is small compared to the width of the pulse height ranges used.

In mapping the line emission, we correct for the underlying continuum, as the continuum may well have a different spatial distribution than the line emission. In a solar abundance plasma, the continua are associated primarily with lower atomic weight atoms and their electrons, and may also include a contribution from a highly energetic, nonthermal population of electrons. Indeed, the X-ray image of Cas A in the line free spectral region of energies between 4-6 keV more closely resembles radio images than it does the line-dominated X-ray broadband image (see Fig. 2, also Holt et al. 1994, Vink et al. 1999, Koralesky et al. 2000, Gotthelf et al. 2000). Because X-ray line and thermal continuum emissivities both scale with the emission measure, the line emission in a region of low surface brightness may still be strong relative to the continuum. To identify ejecta over a wide range of surface brightness, we therefore subtract the continuum from each line image and then form a ratio image relative to the continuum (hereafter referred to loosely as a line equivalent width image, EQW, for brevity). A ratio image of much lower spatial resolution was presented for the Fe K blend in Cas A by Vink et al. (1999).

An optimal continuum subtraction should account for the local shape of the spectrum for a source like Cas A, where the spectrum changes on small spatial scales (Hughes et al. 2000). To do this efficiently, we extracted images in two pulse height bands on either side of that used for the line image (see Fig. 1). These bands minimize the contamination from weak line emission and are in some cases quite narrow, but generally contain over 100,000 counts. The continuum is assumed to be linear throughout the range of pulse heights used for a particular image, and is interpolated pixel by pixel using $1''$ pixels for the Si, S, and Fe L images, and $2''$ for the others. The continuum images for Fe K are sparse, so in this case only, they were simply added and scaled to the appropriate average level inferred from fitting the total spectrum. In the faint regions interior and exterior to the bright broadband shell, some pixels are negative after continuum subtraction, so each raw line and background image is smoothed with a 1-2 pixel gaussian filter before subtraction and division. The final line and line/continuum ratio images are smoothed over 1.5 pixels.

The EQW images for Si, S, Ar, Ca, and Fe (L and K) are shown in Fig. 3. The Si, S, Ar, and Ca images are, on the whole, similar to each other, but notably different from the broadband image and the 4-6 keV continuum. Comparison of the Si EQW image to the intermediate, continuum subtracted Si line image in Fig. 2 shows that the effect of normalizing to the continuum is important. The optical jet to the northeast is strikingly prominent in these EQW images, having EQW intensities comparable to those seen at the bright ejecta shell. Using the Si EQW image to guide the eye, the distribution of Si emission with high EQW is seen to strongly resemble the distribution of fast-moving optical [SII] ejecta knots (e.g., Fesen & Gundersen 1996), including the ring-like structure noted by Lawrence et al. (1995) in the northern arch. It is interesting that the regions just exterior to the bright shell to the north and west in the broadband and Si line images also show high EQW intensities (compare the Si images in Fig. 2 and 3 against the fiducial marker), whereas low EQW Si emission is seen throughout the remnant in regions off the bright shell.

The remnant's eastern boundary in the EQW images of the intermediate mass elements appears more prominent than in the optical, and is closer in to the center of the remnant than in the

broadband X-ray image. The remaining panels of Fig. 3 show that the Fe L and Fe K maps are similar to each other in that their eastern boundaries are exterior to that of the other elements, as previously noted (Hughes et al. 2000, Vink et al. 1999). In addition, Fe emission is weak or absent in the jet region and is contained within the boundary of the bright emission to the north and west seen in other images. We expect a general similarity between the Fe L and K images since Fe K emission is usually accompanied by L emission, but the converse need not be true, and there are regions that are bright in Fe L but not in Fe K; presumably the regions lacking Fe K emission are at lower temperatures. The deficiency of Fe L in the west can be largely attributed to the higher neutral H column density toward this part of the remnant (Keohane et al. 1996), and this also accounts for the weaker Si emission in this region. A final, but important, caveat is that the emission we have identified as “Fe L” may well include a contribution from Ne, an issue to be fully resolved with data of higher spectral resolution.

3. Discussion

It can be verified that the maps in Fig. 3 trace gas that is enriched with supernova ejecta by comparing the observed line intensity ratios to theoretical line/continuum emissivity ratios. Using the approximate Si energy range shown in Fig. 1 for a solar abundance plasma with temperatures between $10^6 - 10^8$ K and ionization ages from $10^9 - 10^{12.4}$ cm^{-3} s, the calculated ratio of the Si line emissivity relative to the continuum does not exceed 2 (and this only at extreme temperatures). A ratio of 2 traces the bright regions of the Si EQW image in Fig. 3, which is consistent with the consensus that the X-ray Si emission in Cas A comes predominantly from ejecta.

A similar calculation for Fe K gives maximum ratios of just over 2 for the same range of parameters, with the highest computed ratios occurring at temperatures of a few keV near collisional ionization equilibrium. A ratio of 2 again outlines the Fe K EQW image in Fig. 3, suggesting that much of this emission may be from ejecta. Another possibility has been suggested by Borkowski et al. (1996), who modelled the Fe K emission in the integrated ASCA spectrum as arising from shocked circumstellar wind material. The images do not rule out the possibility that some of the Fe K emission does come from such a contribution, and to some extent, this could also be true of the emission from Si and other elements. The resolution of this issue requires detailed examination of the spectra, which we defer to future work.

The images in Fig. 3 give a good indication of the distribution of X-ray emitting ejecta, but we emphasize that they do not give detailed abundance information. Theoretical equivalent widths vary with temperature and ionization age, so that a given equivalent width can correspond to significantly different element abundances depending on the local plasma conditions. The EQW maps by themselves should therefore be taken only as an indication of where the abundances are definitely enhanced above the solar value. The details of the maps, particularly in faint emission regions, are moreover dependent on the rather simple assumptions that the local continuum is linear in shape and free of contamination from weak lines, and that the line emission in each image

is due entirely to the element identified. Though this last assumption is likely to be quite valid in most cases, it may not be valid for Fe L, nor would it be for Mg. Finally, the EQW maps by themselves are not actual maps of the ejecta mass, as the mass depends not only on the abundance and emitting volume but also on the local density.

The resemblance between our Si and S line maps and optical maps explicitly demonstrates that the X-ray and optically emitting ejecta are spatially coexistent over much of the remnant. This was anticipated in that the X-ray Si and S line emission, inferred to include a significant contribution from ejecta, show asymmetric Doppler shifts corresponding to bulk velocities of ~ 2000 km/s that are comparable to those of the optical ejecta knots (Markert et al. 1983, Holt et al. 1994). The ejecta in a given region therefore have a wide range of densities and temperatures, and the shocks propagating into the ejecta are highly variable on small scales; the slow shocks required for the optical emission (Reed et al. 1995) cannot explain the X-ray emission.

The faint X-ray jet extends more than $3.5'$ beyond the expansion center used by Kamper & van den Bergh (1976, a position nearly coincident with that of the newly discovered X-ray point source) making it of comparable extent to its optical counterpart. The qualitative resemblance between the X-ray image of the jet and the optical images of Fesen & Gunderson (1996) is striking. In particular, the three prominent filaments of the outer optical jet and the triangular shaped base are all seen to have X-ray counterparts. Our maps also show that the abundances of Si and S are enhanced in faint regions just outside the bright shell in the north and west, but they do not reveal any other extended region of enhanced abundance comparable to the northeast jet. The Si image, containing the highest number of photons, does show faint streamers of emission extending radially outward directly opposite the jet to the west, but with a larger opening angle, and with equivalent widths that are not high enough to indicate unambiguously that these are ejecta.

We have noted that Si, S, Ar, and Ca have similar general morphologies, but examination of the individual panels of Fig. 3 does show differences between them. A detailed survey of such differences is beyond the scope of this paper, but two notable examples are the brightest knots in the Si image of Fig. 2, at the inner boundary of the shell to the northeast and southeast: these are much weaker in the Ar and Ca EQW maps than in Si and S. The southeast knot was analyzed qualitatively by Hughes et al. (2000), and it appears that the Ar and Ca abundances here are indeed lower, and that these ejecta originate in an outer ejecta zone compared to knots with strong emission for all four elements.

The overall difference between the Si and Fe EQW maps in the east appears to support the suggestion that the inner Fe ejecta layers have been overturned and propelled beyond the Si ejecta layers in this part of the remnant, and may be related to the asymmetries that created the jet nearby. Such overturning of ejecta layers was first suggested by Chevalier & Kirshner (1979 and references therein) to explain the properties of the optical knots, and also occurs in recent models (e.g., Kifonidis et al. 2000, Khokhlov et al. 1999).

In summary, the X-ray line maps presented in this paper reveal the spatial striking corre-

spondence between the optically and X-ray emitting ejecta in Cas A, explicitly showing that the different physical conditions giving rise to each coexist on small spatial scales.

We thank Paul Plucinsky for expert advice during the planning of this observation, and Harvey Tananbaum for gracious assistance in scheduling it.

REFERENCES

- Borkowski, K. J., Szymkowiak, A. E., Blondin, J. M., & Sarazin, C. L. 1996, *ApJ*, 466, 866
- Chevalier, R. A., & Kirshner, R. P. 1979, *ApJ*, 233, 154
- Fesen, R. A., & Gundersen, K. S. 1996, *ApJ*, 470, 967
- Fujimoto, R., et al. 1995, *PASJ*, 47, L31
- Gotthelf, E. V., et al. 2000, in preparation
- Holt, S. S., Gotthelf, E. V., Tsunemi, H., & Negoro, H. 1994, *PASJ*, 46, L151
- Hwang, U., & Gotthelf, E. V. 1997, *ApJ*, 475, 665
- Hughes, J. P., Rakowski, C. E., Burrows, D. N., & Slane, P. O. 2000, *ApJL*, 528, L109
- Kamper, K. W., & van den Bergh, S. 1987, *ApJS*, 32, 351
- Keohane, J. W., Rudnick, L., & Anderson, M. C. 1996, *ApJ*, 466, 309
- Khokhlov, A. M., Höflich, P. A., Oran, E. S., Wheeler, J. C., Wang, L., & Chtchelkanova, A. Yu. 2000, *ApJL*, 524, L107
- Kifonidis, K., Plewa, T., Janka, H.-Th., & Müller, E., 2000, *ApJL*, 531, L123
- Koralesky, B., et al. 2000, in preparation
- Lawrence, S. S., et al. 1995, *AJ*, 109, 2635
- Markert, T. H., Canizares, C. R., Clark, G. W., & Winkler, P. F. 1983, *ApJ*, 268, 134
- Reed, J. E., Hester, J. J., Fabian, A. C., & Winkler, P. F. 1995, *ApJ*, 440, 706
- Vink, J., Concetta Maccarone, M., Kaastra, J. S., Mineo, T., Bleeker, J. A. M., Preite-Martinez, A., Bloemen, H. 1999, *A&A*, 344, 289

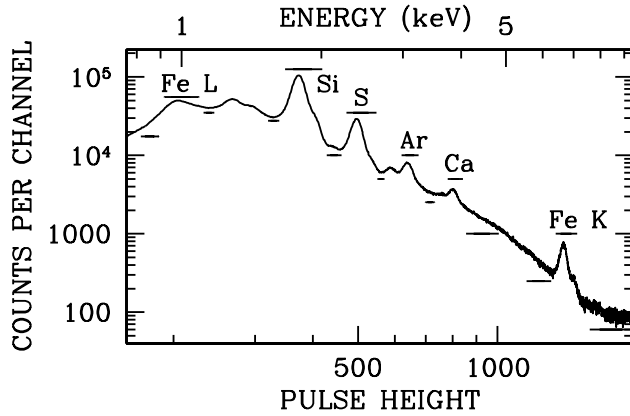


Fig. 1.— The ACIS spectrum of Cas A plotted against both pulse height and energy (using an approximate gain value of 4.8 eV per channel). Horizontal bars above the spectrum show the pulse height intervals used for each image, also labelled by element; bars below the spectrum show the neighboring intervals used for the continua.

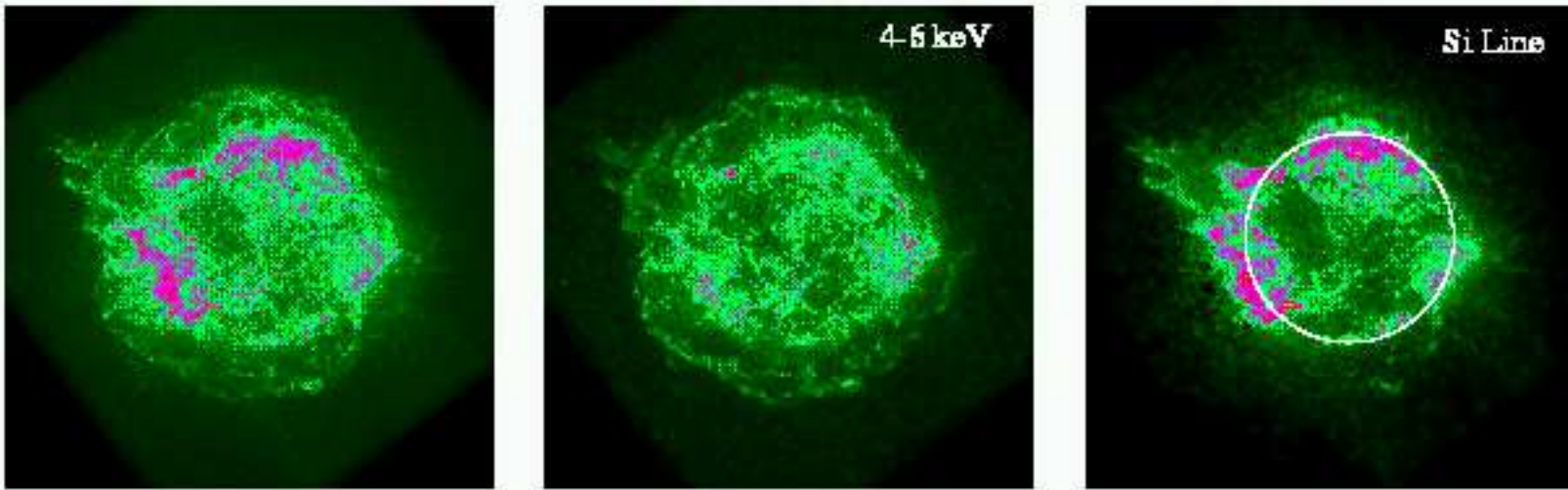


Fig. 2.— (Left) The broadband ACIS S3 image of Cas A. (Middle) The 4-6 keV continuum image. (Right) The continuum-subtracted Si line image with a fiducial circle of radius 1.8 arcmin overlaid. All images are 512 arcsec across with square-root intensity scales.

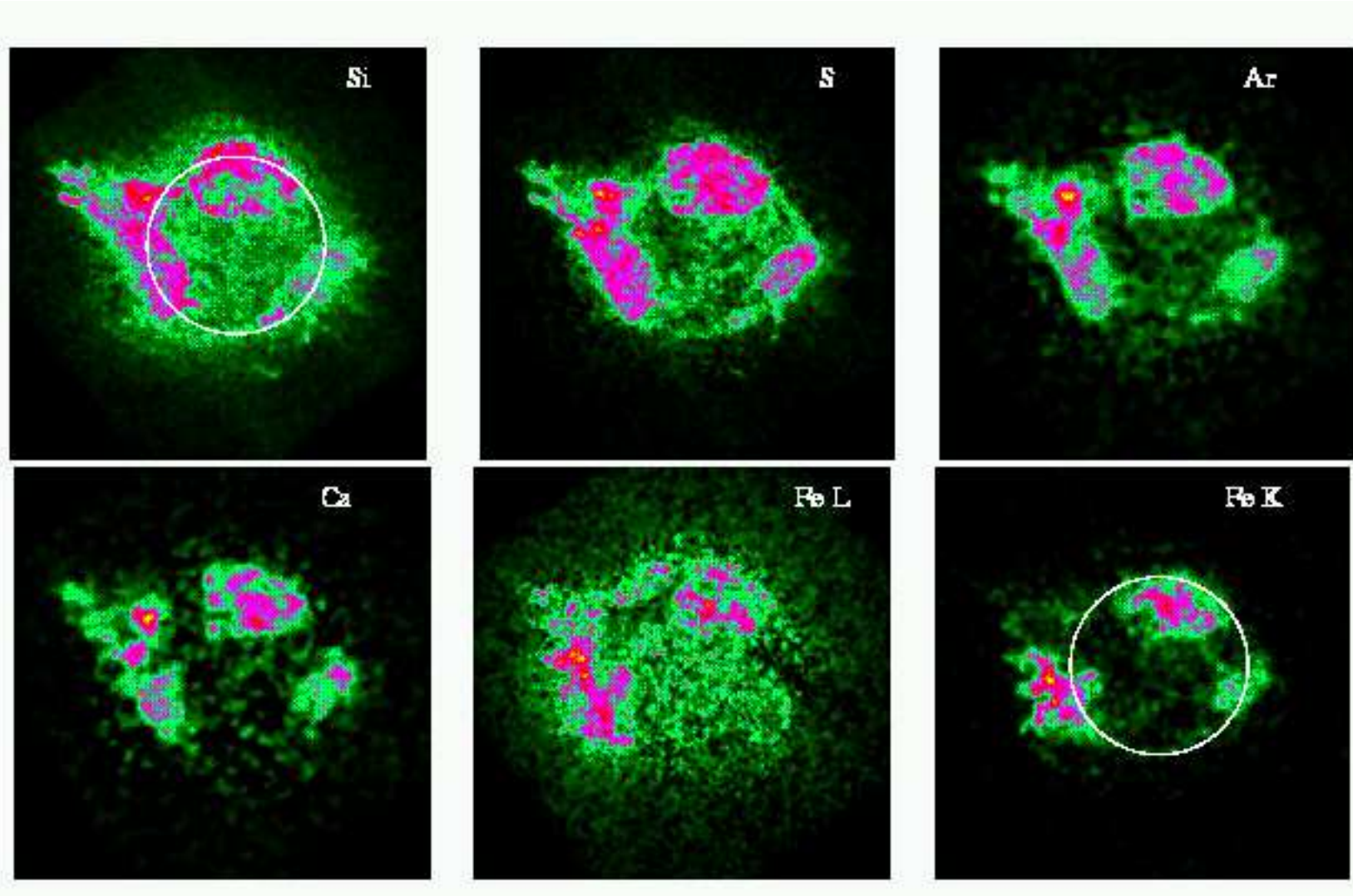


Fig. 3.— Left to right: Line-to-continuum ratio (equivalent width) images for (top) Si, S, Ar, (bottom) Ca, Fe L, and Fe K. The same fiducial circle in Fig. 2 is overlaid on the Si and Fe K images to facilitate comparisons; the intensity scales are linear and negative ratios have been set to zero.